nature medicine

ARTICLES

https://doi.org/10.1038/s41591-018-0036-4

Monocyte-derived IL-1 and IL-6 are differentially required for cytokine-release syndrome and neurotoxicity due to CAR T cells

Margherita Norelli[1,2], Barbara Camisa[1], Giulia Barbiera[3], Laura Falcone[1], Ayurzana Purevdorj[1], Marco Genua[3], Francesca Sanvito[4], Maurilio Ponzoni[4], Claudio Doglioni[4], Patrizia Cristofori[5], Catia Traversari[6], Claudio Bordignon[2,6], Fabio Ciceri[2,7], Renato Ostuni[3], Chiara Bonini[2,8], Monica Casucci[1] and Attilio Bondanza[1,2*]

In the clinic, chimeric antigen receptor–modified T (CAR T) cell therapy is frequently associated with life-threatening cytokine-release syndrome (CRS) and neurotoxicity. Understanding the nature of these pathologies and developing treatments for them are hampered by the lack of appropriate animal models. Herein, we describe a mouse model recapitulating key features of CRS and neurotoxicity. In humanized mice with high leukemia burden, CAR T cell–mediated clearance of cancer triggered high fever and elevated IL-6 levels, which are hallmarks of CRS. Human monocytes were the major source of IL-1 and IL-6 during CRS. Accordingly, the syndrome was prevented by monocyte depletion or by blocking IL-6 receptor with tocilizumab. Nonetheless, tocilizumab failed to protect mice from delayed lethal neurotoxicity, characterized by meningeal inflammation. Instead, the IL-1 receptor antagonist anakinra abolished both CRS and neurotoxicity, resulting in substantially extended leukemia-free survival. These findings offer a therapeutic strategy to tackle neurotoxicity and open new avenues to safer CAR T cell therapies.

Genetically engineering T cells modified with CARs represents a highly sophisticated and radically innovative method for treating cancer. The basic structure of a CAR usually comprises a tumor-targeting domain derived from a monoclonal antibody fused to the CD3 zeta chain and a CD28 (refs [1–3]) or a 4-1BB[4,5] costimulatory endodomain. In first-in-man studies, CD19-specific CAR T cells showed remarkable antitumor efficacy against B cell malignancies. More recently, two distinct Food and Drug Administration (FDA) approvals have paved the way to a wider clinical availability of CD19 CAR T cell therapy[6,7]. Unfortunately, this unprecedented efficacy is accompanied by long-lasting B cell aplasia, and most importantly, by severe CRS. Clinical manifestations of severe CRS (high fever, increased levels of acute-phase proteins and respiratory and cardiovascular insufficiency) typically develop within the first days after infusion and, if left untreated, may lead to death[8]. Recognized factors for life-threatening CRS are tumor burden[8] and in vivo peak expansion of CAR T cells promoted by prior lymphodepletion[9,10]. CRS responsiveness to the anti-IL-6 receptor (IL-6R) monoclonal antibody tocilizumab as well as correlative biomarker studies[8,11] point to a key role for IL-6 signaling in the pathogenesis of this syndrome. A revised grading system has been also proposed with the aim of prospectively identifying patients at high risk for severe CRS and for guiding targeted interventions[12].

Another increasingly reported toxicity by CD19 CAR T cells involves the central nervous system (CNS). Signs of neurological dysfunction often develop during CRS but usually subside after its resolution. Nonetheless, a delayed and potentially lethal form of neurotoxicity has been reported days to weeks after disappearance of CRS signs[7,9,13]. Interestingly, neurotoxicity by CD19 CAR T cells is seemingly more frequent in acute lymphoblastic leukemia (ALL) and, at odds with initial conjectures, appears to occur independently from leukemic CNS localization. As neurotoxicity is also frequently observed with the CD19–CD3-bispecific monoclonal antibody blinatutomab[14], some authors have speculated that neurotoxicity might be, for some reasons, specifically linked to the CD19 target antigen. Interestingly preliminary clinical experience suggests that, although effective in CRS management, tocilizumab may fail at preventing delayed neurotoxicity[9,13].

Currently available preclinical xenograft mouse models are poorly predictive of the clinical behavior of CAR T cells owing to the lack of bystander human hematopoiesis and to the almost invariant development of xenogeneic graft-versus-host disease (X-GVHD)[15,16]. Most importantly, these models fail at reproducing severe CRS and lethal neurotoxicity, and as tocilizumab does not cross-react with mouse IL-6R, it cannot be used to address potential hindrance with antitumor efficacy. In this study, we have established a new xenotolerant mouse model recapitulating all major toxicities induced by CD19 CAR T cells in humans, including long-lasting B cell aplasia, severe CRS and lethal neurotoxicity, and we took advantage of this model to shed new light on the mechanisms underlying these toxicities. The results obtained address fundamental questions in the CAR T cell field, such as whether similar toxicities are observed with other antigens besides CD19, whether pharmacological prophylaxis or treatment hampers antileukemic

[1]Innovative Immunotherapies Unit, San Raffaele Hospital Scientific Institute, Milano, Italy. [2]Vita-Salute San Raffaele University, Milano, Italy. [3]Genomics of the Innate Immune System Unit, San Raffaele-Telethon Institute for Gene Therapy (SR-Tiget), Milano, Italy. [4]Pathology Unit, San Raffaele Hospital Scientific Institute, Milano, Italy. [5]San-Raffaele-Telethon Institute for Gene Therapy (SR-Tiget), Milano, Italy. [6]Molmed Spa, Milano, Italy. [7]Hematology and Bone Marrow Transplantation Unit, San Raffaele Hospital Scientific Institute, Milano, Italy. [8]Experimental Hematology Unit, San Raffaele Hospital Scientific Institute, Milano, Italy. *e-mail: attilio.bondanza@gmail.com

© 2018 Nature America Inc., part of Springer Nature. All rights reserved.

efficacy and whether neurotoxicity can be managed effectively. Throughout the study, we used CAR T cells specific for CD44v6, an antigen overexpressed on acute myeloid leukemia (AML) and multiple myeloma (MM)[17] as well as on circulating monocytes for comparison with CD19 CAR T cells.

Results

Nonxenoreactive nHuSGM3 T cells can be CAR redirected. Aiming at the development of a xenograft mouse model for studying the specific contribution of myeloid cells to the toxicities of CAR T cells, we transplanted human cord blood (CB) hematopoietic stem and progenitor cells (HSPCs) through intrahepatic injection into sublethally irradiated newborn NSG or triple transgenic NSG (SGM3) mice expressing human stem cell factor, granulocyte-macrophage colony-stimulating factor (GM-CSF) and IL-3 and initially profiled lymphohematopoietic reconstitution. Compared with newborn humanized NSG (HuNSG) mice, newborn humanized SGM3 (HuSGM3) mice reconstituted hematopoiesis more rapidly and with higher counts of human B cells, monocytes and T cells as well as cells from other lineages (Fig. 1a–c and Supplementary Fig. 1b–d). The timing of HSC injection soon after birth was critical for successful human T lymphopoiesis, as a 2-d delay almost completely dampened the effect (Supplementary Fig. 2a). For the rest of this study, we will refer to SGM3 mice reconstituted with human HSPCs at the newborn stage as nHuSGM3 mice. Circulating T cells in nHuSGM3 mice displayed a physiological CD4/CD8 ratio and over time appeared to differentiate from CD45RA$^+$CD62L$^+$ naive (T_{Na}) to CD45RA$^-$CD62L$^+$ central memory (T_{CM}) to CD45RA$^-$CD62L$^-$ effector memory (T_{EM}) cells (Supplementary Fig. 2b,c). Only a minority of CD45RA$^+$CD62L$^+$ T cells expressed the stem cell memory (T_{SCM}) marker CD95[18] (Supplementary Fig. 2d). T cell development in nHuSGM3 mice was associated with substantial thymus cellularity, including single-positive CD4 or CD8 T cells (Supplementary Fig. 2e) and an architecture characterized by distinct cortical and medullary areas (Fig. 1d) that were populated with human CD3$^+$ T cells, as determined by immunohistochemistry (Fig. 1e). Spleen and bone marrow were also colonized by human T cells (Supplementary Fig. 2f,g).

Intrigued by the observation of sizeable T lymphopoiesis in nHuSGM3 mice, we next characterized the functionality of these T cells. In vitro, nHuSGM3 T cells were hyporesponsive to NSG mouse antigens (I-A^{g7}) but vigorously proliferated in response to C57/Bl6 mouse antigens (I-A^d) and to human alloantigens (Fig. 1f). Moreover, once intravenously (i.v.) transferred into sublethally

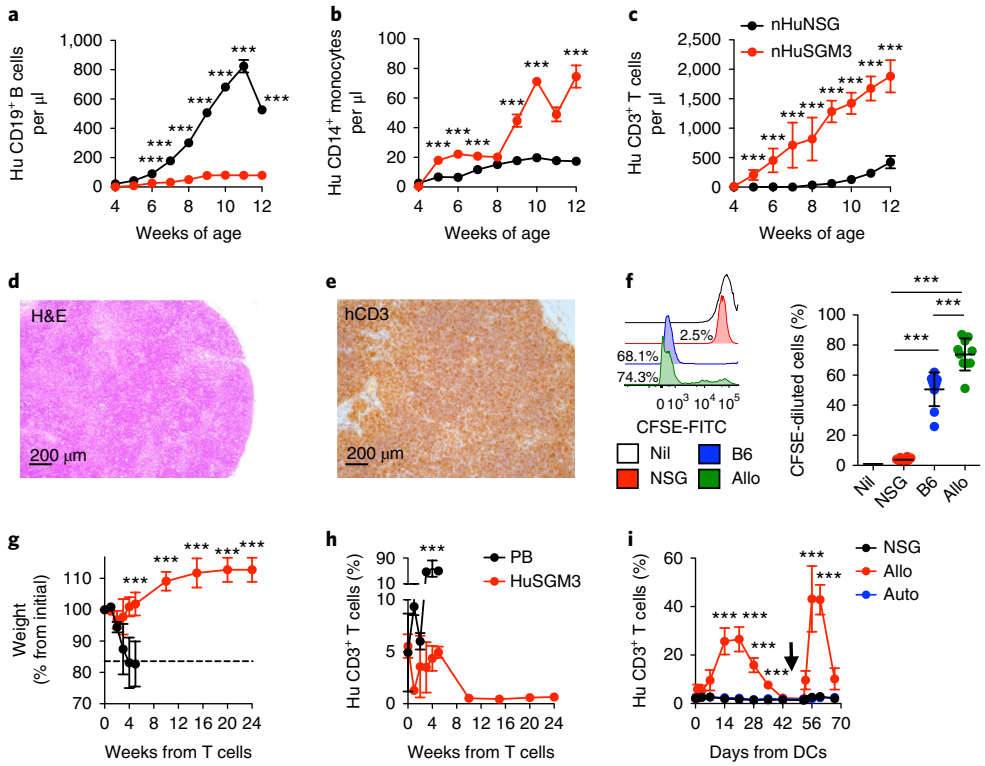

Fig. 1 | HuSGM3 T cells are nonxenoreactive and can be CAR redirected. Human HSPCs ($n=4$ donors) were intrahepatically injected into irradiated newborn NSG (nHuNSG, $n=10$) or SGM3 (nHuSGM3, $n=10$) mice. **a**–**c**, Mean counts ± s.d. of human (Hu) CD19$^+$ B cells (**a**), CD14$^+$ monocytes (**b**) and CD3$^+$ T cells (**c**) in nHuNSG and nHuSGM3 mice. A two-way ANOVA was used for statistical analysis; ***$P<0.001$. **d**,**e**, H&E (**d**) and human CD3 immunohistochemistry (**e**) images of nHuSGM3 thymus at 12 weeks of age (representative of $n=5$ mice). **f**, T cells were harvested from the spleens of 12-week-old nHuSGM3 mice and were left unstimulated (Nil, $n=10$ from 5 independent experiments) or were cocultured with irradiated splenocytes from NSG ($n=10$) or C57/Bl6 (B6, $n=10$) mice or with irradiated human allogeneic mononuclear cells (Allo, $n=10$). Proliferation of HuSGM3 T cells was measured through carboxyfluorescein succinimidyl ester (CFSE) dilution. A representative plot (left) and percentages ± s.d. of cells diluted through CFSE (right) are shown. A one-way ANOVA was used for statistical analysis; ***$P<0.001$. **g**,**h**, 5×10^6 nHuSGM3 or human T cells were infused i.v. into sublethally irradiated NSG mice ($n=15$ per group from 3 independent experiments). Mean weight change ± s.d. of mice (**g**) and frequency of human CD3$^+$ T cells in mouse blood ± s.d. (**h**) are shown. **i**, 5×10^6 nHuSGM3 T cells were transferred into sublethally irradiated NSG mice ($n=18$ from 2 independent experiments). After 24 weeks, mice were challenged with irradiated DCs from NSG mice (NSG, $n=6$), human allogeneic peripheral blood mononuclear cells (Allo, $n=6$) or autologous CB mononuclear cells (Auto, $n=6$). Mice were rechallenged after 48 d (arrow). Mean percentages ± s.d. of circulating human CD3$^+$ T cells out of all human T cells are shown. For **g**–**i**, a two-way ANOVA was used for statistical analysis; ***$P<0.001$.

© 2018 Nature America Inc., part of Springer Nature. All rights reserved.

irradiated secondary NSG recipients, nHuSGM3 T cells failed to induce X-GVHD, yet they persisted at low levels for up to 24 weeks (Fig. 1g,h). The functionality of nHuSGM3 T cells transferred in vivo was confirmed by expansion in response to vaccination with human allogeneic dendritic cells (DCs), but not with autologous CB-derived or NSG mouse DCs (Fig. 1i). T cells isolated from nHuSGM3 mice were transduced with anti-CD44v6 CARs of different designs (28z, BBz, zOX). Transduction and expansion rates with these CARs were lower than that of T cells from human peripheral blood (PB) but were comparable to those of CB-derived T cells (Supplementary Fig. 3a,b). The CD4/CD8 ratio and memory differentiation phenotypes were unaffected by CAR transduction (Supplementary Fig. 3c,d). nHuSGM3 T cells transduced with the CD44v6.28z or CD44v6.zOX CAR, but not with the CD44v6.BBz CAR, killed the CD44v6$^+$ THP-1 leukemia cell line in vitro (Supplementary Fig. 4a). CD44v6.BBz CAR T cells from human PB were also less effective in comparison to CD44v6.28z- or CD44v6.zOX-transduced cells (Supplementary Fig. 4d–f), indicating that suboptimal functionality was due to this particular design rather than to T cell source. Accordingly, there was no difference in killing activity between the CD19.28z and CD19.BBz designs (Supplementary Fig. 4g–i). Once infused i.v. into mice previously engrafted with THP-1 leukemic cells, CD44v6.28z CAR T cells from nHuSGM3 mice were as potent as those from human PB in controlling leukemic outgrowth (Supplementary Fig. 5a–d). Moreover, nHuSGM3 CAR T cells were progressively enriched for transgene expression, confirming the lack of xenoreactivity (Supplementary Fig. 5e).

Leukemia clearance by nHuSGM3 CAR T cells causes cytokine-release syndrome. To evaluate the efficacy of CAR T cells specific for CD19 and CD44v6 in vivo against the same target cells, we transduced the patient-derived CD19$^+$ ALL-CM leukemia cell line[19] with different CD44 isoforms containing or not containing the variant 6 (Supplementary Fig. 6a,b). After initial remission, CD44v6$^+$CD19$^+$ ALL-CM leukemia–bearing mice infused with CD44v6.BBz CAR T cells eventually relapsed, whereas those that received CD44v6.28z, CD19.BBz or CD19.28z CAR T cells benefited from durable antileukemic effects (Supplementary Fig. 6c,d). For sake of comparability, all subsequent experiments were performed with either CD19.28z or CD44v6.28z CAR T cells.

To study early toxicities associated with CAR T cell antileukemic effects, adult SGM3 mice were infused with ALL-CM leukemic cells and later with CD19.28z or CD44v6.28z CAR T cells, either after 5 or 7 weeks following ALL-CM infusion (low or high leukemia burden, respectively; Supplementary Fig. 7a,b). Even if CD44v6.28z or CD19.28z CAR T cells mediated rapid and long-lasting leukemia clearance in PB in both settings, CAR T cells robustly expanded in vivo only in the case of high leukemia burden (Supplementary Fig. 7c,d), and mice developed a transient syndrome (median duration, 7 d; range, 3–10 d) that was characterized by moderate weight loss, mild fever and increased systemic levels of human interferon (IFN)-γ and IL-2 but not of tumor necrosis factor (TNF)-α, IL-10 and IL-6 (Supplementary Fig. 7e–h). Levels of serum amyloid A (SAA), a murine homolog to the human CRS biomarker C-reactive protein[8] whose production is under IL-6 control, were also unchanged (Supplementary Fig. 7i), whereas uric acid transiently rose (Supplementary Fig. 7j), suggesting the development of tumor-lysis syndrome rather than CRS. Long-term antileukemic efficacy by CAR T cells was confirmed by high rates of deep remission (bone marrow leukemic cells < 5%; Supplementary Fig. 7k) at 24 weeks from infusion, without differences between mice infused with CD19.28z (7 of 11 mice) or CD44v6.28z (5 of 11 mice) CAR T cells. The 5% cut-off for deep remission was chosen on the basis of lack of engraftment in tertiary recipients (Supplementary Fig. 7l,m).

Endogenous myeloid cells from immunocompromised mice derived from the NOD background are known to be functionally defective[20–22]. Aiming at modeling human CRS, we therefore infused nHuSGM3 CAR T cells into secondary HuSGM3 recipients as a way to simultaneously provide functional myeloid cells (Fig. 2a) and antigenic CD19$^+$ B cells or CD44v6$^+$ monocytes (Supplementary Fig. 8a). As expected, CD19.28z and CD44v6.28z CAR T cells expanded in vivo, although with different kinetics (Supplementary Fig. 8b), and induced long-lasting B cell and monocyte aplasia (Fig. 2b,c), respectively. Moreover, despite a substantial difference in circulating antigenic cells before infusion, CD19.28z and CD44v6.28z CAR T cells equivalently caused a violent systemic inflammatory syndrome, highly reminiscent of human CRS and characterized by severe weight loss, increased systemic human IL-6 levels and high fever (Fig. 2d–f). Elevations of systemic human TNF-α and IL-10 (Supplementary Fig. 8c,d), as well as of mouse SAA (Fig. 2g), closely mirrored the kinetics of the syndrome. All these signs were absent in SGM3 mice (not previously humanized with HSCs). Interestingly, it was evident that CRS induced by CD44v6.28z CAR T cells was somewhat earlier and shorter than that by CD19.28z CAR T cells, although they both resulted in comparable mortality (25% versus 33.3%). As determined through histopathology, mice dying from CRS had human CAR T cell infiltration in the liver that was often accompanied by a human histiocytic component (data not shown).

Monocytes are major sources of IL-1 and IL-6 during cytokine-release syndrome. We next examined whether leukemia presence, and especially the amount of circulating leukemic cells, in HuSGM3 mice could be a determinant of CRS severity by CAR T cells, as is observed in humans[7,9,13]. For this aim, SGM3 mice were coengrafted with human HSPCs and ALL-CM leukemic cells and, after verifying the establishment of different leukemia burdens, were infused with nHuSGM3 CAR T cells (Fig. 3a). CRS following either CD19.28z or CD44v6.28z CAR T cell infusion was more severe in the case of high leukemia burden as revealed by more profound weight loss, higher systemic levels of human IL-6 (Supplementary Fig. 9a–d), fever (Fig. 3b,c) and markedly increased mortality (Fig. 3d,e) in recipient mice. Severe CRS correlated with in vivo kinetics of CAR T cells (Supplementary Fig. 9e,f) and with systemic human interferon (IFN)-γ elevation (Supplementary Fig. 9g,h). During CRS, the majority of mouse cytokines and chemokines tested were undetectable (Supplementary Fig. 9i), suggesting they only had a minor contribution, if any, to the observed effects. Leukemic HuSGM3 mice infused with irrelevant EGFR.28z CAR T cells as control did not develop CRS (Supplementary Fig. 10a–e) but died from leukemia within 8 weeks (Supplementary Fig. 10f).

To determine whether the CAR costimulatory endodomain influences CRS, we compared its incidence and severity caused by nHuSMG3 T cells transduced with either 28z or BBz CAR specific for CD19 or CD44v6 adoptively transferred into HuSGM3 recipients with high leukemia burden. CD44v6.BBz CAR T cells expanded with different kinetics (Fig. 3f) and unexpectedly caused significantly more severe CRS than CD44v6.28z CAR T cells, resulting in 100% mortality (Fig. 3g,h). Despite greater T cell activation in vivo (Supplementary Fig. 11a), CD44v6.BBz CAR T cells mediated inferior antileukemic effects and a paradoxical surge in human monocyte counts (Supplementary Fig. 11b,c). Such an effect was mirrored by increased systemic levels of human inflammatory cytokines (Supplementary Fig. 11d–g) and, among monocyte-derived chemokines, of CCL3 (also called MIP-1α) (Supplementary Fig. 11h–k). In line with results in humans[7,13], CD19.BBz CAR T cells mediated similar antileukemic effects compared to CD19.28z CAR T cells without inducing overwhelming mortality (Fig. 3i–k).

In this model, monocyte numbers accumulate concomitantly with leukemia progression. Thus, mice receiving CAR T cells at 7 weeks following HSPC and leukemia infusion had higher

© 2018 Nature America Inc., part of Springer Nature. All rights reserved.

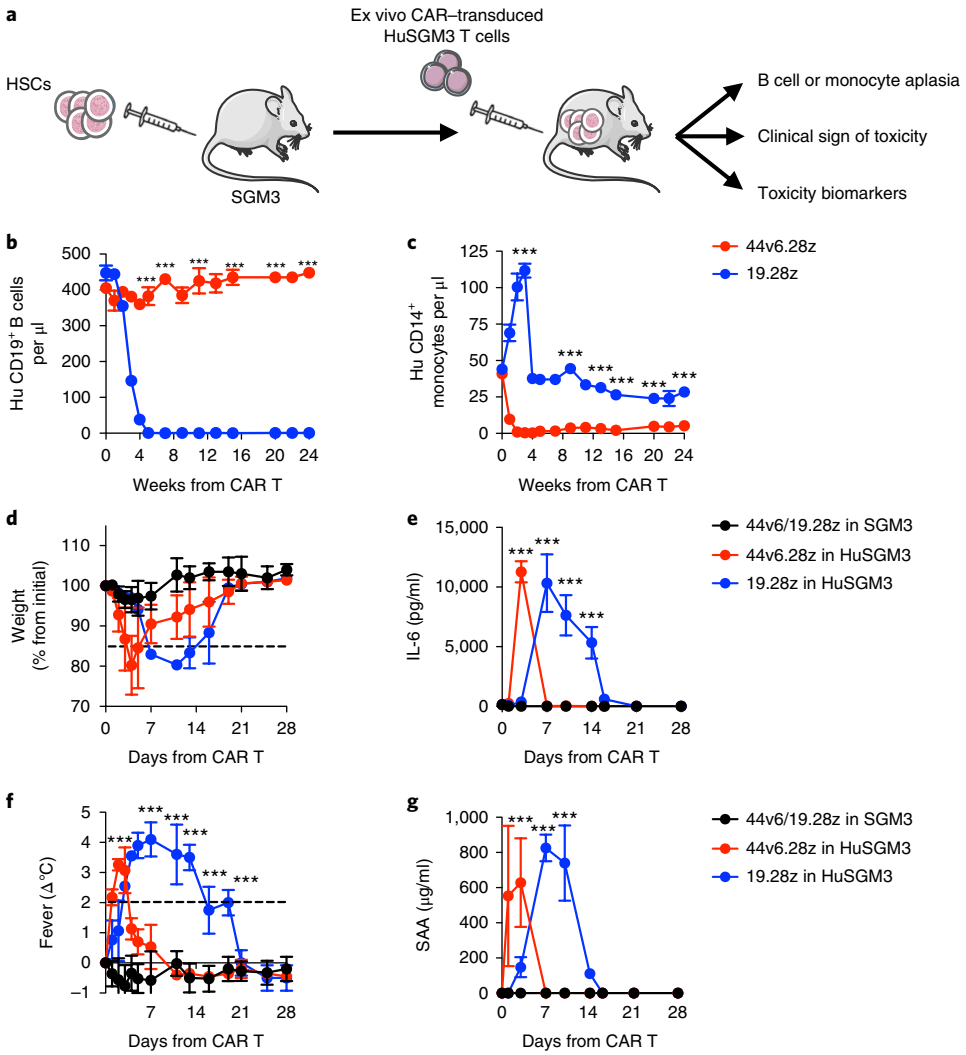

Fig. 2 | CAR T cells cause CRS in HuSGM3 mice. a, Eight-week-old SGM3 mice were infused i.v. with 1×10^5 HSPCs ($n=3$ donors, HuSGM3). Four weeks after that, they were infused with 2×10^6 T cells from nHuSGM3 mice transduced with either a CD44v6.28z CAR (44v6.28z in HuSGM3, $n=15$ from 3 independent experiments) or a CD19.28z CAR (19.28z in HuSGM3, $n=15$). Non-HSPC-humanized SGM3 mice (not shown in the schematic) were infused with either nHuSGM3 CD44v6.28z or CD19.28z CAR T cells as control, and results were pooled (44v6/19.28z in SGM3, $n=18$). **b**,**c**, Mean counts ± s.d. of human CD19+ B cells (**b**) and CD14+ monocytes (**c**) following CAR T infusion. A two-way ANOVA with Bonferroni correction was used for statistical analysis; ***$P<0.001$. **d**, Mean weight change ± s.d. following CAR T infusion. Dashed lines indicate the threshold for severe weight loss (>15%). **e**, Mean human IL-6 serum concentration ± s.d. A two-way ANOVA was used for statistical analysis; ***$P<0.001$. **f**, Mean body temperature change ± s.d. Dashed lines indicate the threshold for high fever (change in temperature (ΔT) > 2 °C). A two-way ANOVA with Bonferroni correction was used for statistical analysis; ***$P<0.001$. **g**, Mean mouse SAA concentrations ± s.d. A two-way ANOVA with Bonferroni correction was used for statistical analysis; ***$P<0.001$.

monocyte counts in blood than mice treated with CAR T cells at 5 weeks. To weigh the contribution of monocytes to CRS, we took advantage of the observation that their reconstitution in HSPC-humanized mice is strain- and sex-dependent (Fig. 4a), whereas leukemia engraftment and CAR T cell kinetics (Supplementary Fig. 12a,b) are not. CRS mortality by CD19.28z CAR T cells proved higher in female HuSGM3 than in female HuNSG mice (Fig. 4b), correlating with monocyte counts. More directly, depleting monocytes before CD19.28z CAR T cell infusion by liposomal clodronate administration (Supplementary Fig. 12c) had no direct effect on B cell or leukemic cell (Supplementary Fig. 12d,e) counts, yet this completely abated CRS incidence and mortality (Fig. 4c,d and Supplementary Fig. 12g). However, after a closer look, it was evident that monocyte depletion had a negative impact on in vivo CAR T cell expansion (Supplementary Fig. 12f) and on the kinetics of leukemia clearance (Fig. 4e). Similar results were observed with CD44v6.28z CAR T cells (Supplementary Fig. 12h–j). The adjuvant role of monocytes on leukemia elimination by CD19.28z CAR T cells was confirmed in vitro in three-party coculture experiments (Supplementary Fig. 13a).

To demonstrate that monocytes were primarily responsible for CRS and that they contributed to the antileukemic effects by CAR T cells, we used CD44v6.28z CAR T cells to ablate monocytes long-term in HuSGM3 mice and subsequently challenged them with leukemia. In agreement with our hypothesis, mice rendered monocyte-aplastic by prophylactic CD44v6.28z CAR T cells, but not mice infused with CD19.28z CAR T cells as control, were protected from CRS (Fig. 4f,g and Supplementary Fig. 13b). In the absence of monocytes, decreased secondary in vivo expansion of CD44v6.28z compared to CD19.28z CAR T cells (Supplementary Fig. 13c) was, however, associated with higher BM leukemia residual disease (Fig. 4h).

© 2018 Nature America Inc., part of Springer Nature. All rights reserved.

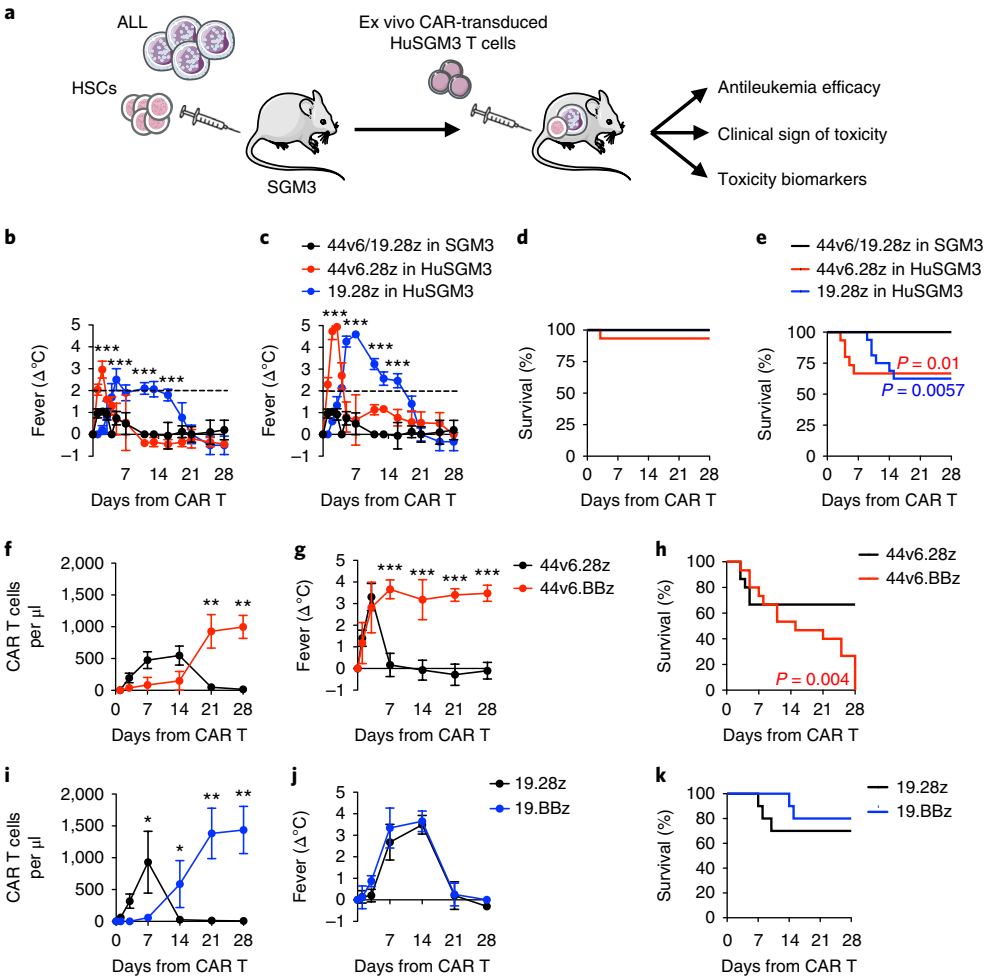

Fig. 3 | CRS severity correlates with leukemia burden. a, Eight-week-old SGM3 mice were co-infused i.v. with 1×10^5 HSPCs ($n=3$ donors, HuSGM3) and 5×10^6 CD19$^+$CD44v6$^+$ ALL-CM leukemic cells, and, after either 4 weeks (low leukemia burden) or 7 weeks (high leukemia burden), with nHuSGM3 T cells transduced with either a CD44v6.28z CAR (44v6.28z, $n=15$ from 3 independent experiments) or a CD19.28z CAR (19.28z, $n=15$). Leukemic non-HSPC-humanized SGM3 mice were infused with either nHuSGM3 CD44v6.28z or CD19.28z CAR T cells as control, and results were pooled (44v6/19.28z in SGM3, $n=18$). **b**,**c**, Mean temperature change ± s.d. in mice with low (**b**) and high (**c**) leukemia burden. Dashed lines indicate the threshold for high fever ($\Delta T>2$ °C). A two-way ANOVA with Bonferroni correction was used for statistical analysis; ***$P<0.001$. **d**,**e**, Kaplan–Meyer survival plots for mice with low (**d**) and high (**e**) leukemia burden. Results from a Mantel–Cox two-sided log-rank test are shown as exact P values for 44v6.28z in HuSGM3 versus 44v6/19.28z in SGM3 (red; hazard ratio, 10.3; 95% confidence interval (CI), 1.7–61.3) or for 19.28z in HuSGM3 versus 44v6/19.28z in SGM3 (blue; hazard ratio: 9.8; 95% CI, 1.9–49.9). **f–k**, HuSGM3 mice with high leukemia burden were infused with nHuSGM3 T cells transduced with either a CD44v6.28z CAR (44v6.28z, $n=10$ from 2 independent experiments), a CD44v6.BBz CAR (44v6.BBz, $n=10$), a CD19.28z CAR (19.28z, $n=10$) or a CD19.BBz CAR (19.BBz, $n=10$). Mean CAR T cell counts ± s.d. (**f**,**i**) and mean temperature change ± s.d. (**g**,**j**) are shown. Dashed lines indicate the threshold for high fever ($\Delta T>2$ °C). A two-way ANOVA with Bonferroni correction was used for statistical analysis; *$P<0.05$; **$P<0.01$; ***$P<0.001$. Kaplan–Meyer survival plots for mice (**h**,**k**) are also shown. Exact P values from a Mantel–Cox two-sided log-rank test are shown for 44v6.BBz versus 44v6.28z (red; hazard ratio, 0.3; 95% CI, 0.1–0.6).

Although IL-6 is recognized as pivotal for CRS pathogenesis[11], it is at present unknown whether CAR T cells are its major source. To address this issue, we set up an in vitro cytokine-release assay by coculturing CD19.28z or control EGFR.28z CAR T cells with leukemic cells with or without THP-1 leukemic cells differentiated into monocyte-like cells (mTHP-1). In this assay, although GM-CSF and TNF-α (Supplementary Fig. 14a,b) were released upon specific tumor recognition by CD19.28z CAR T cells alone, the production of IL-1, IL-6, IL-8 and CCL3/MIP-1α required mTHP-1 (Supplementary Fig. 14c–f). Interestingly, a time-course analysis revealed that IL-1 preceded IL-6 release by approximately 24 h (Supplementary Fig. 14g). Intracellular staining results confirmed the kinetics of IL-1 and IL-6 production both in vitro using primary autologous monocytes (Supplementary Fig. 15a,b) and in vivo in leukemic HuSGM3 mice infused with CD19.28z (Fig. 5a,b), but not with control EGFR.28z, CAR T cells (Supplementary Fig. 15c,d). In vivo, transient IL-6 production was also detected in CD19.28z CAR T cells, but this was limited to the CD4 subset (Supplementary Fig. 15e).

To define the cellular determinants of CRS in an unbiased manner, we performed single-cell RNA-sequencing (scRNA-seq) on whole human CD45$^+$ leukocytes isolated from leukemic HuSGM3 mice infused with CD19.28z CAR T cells at 2 and 7 d after fever onset. Clustering analysis identified 12 clusters encompassing the major human lymphoid and myeloid cell populations (Fig. 5c, Supplementary Fig. 16c–g and Supplementary Table 2). Cell populations showed different dynamics during CRS (Supplementary Fig. 16h). Monocytes and DCs were detected at

© 2018 Nature America Inc., part of Springer Nature. All rights reserved.

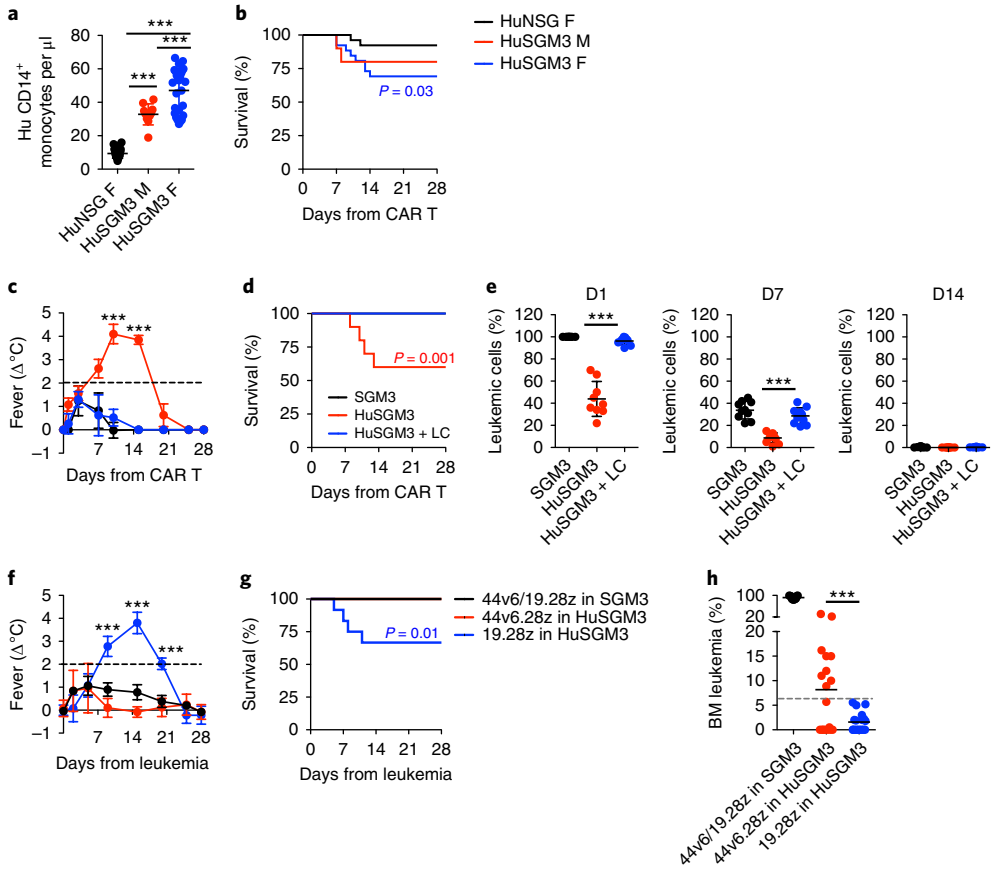

Fig. 4 | Monocyte ablation protects HuSGM3 mice from CRS. a,**b**, Eight-week-old female NSG (HuNSG F, $n=26$ from 3 independent experiments) mice, male SGM3 (HuSGM3 M, $n=10$) or female SGM3 (HuSGM3 F, $n=26$) mice were co-infused i.v. with 1×10^5 HSPCs ($n=3$ donors) and 5×10^6 CD19$^+$CD44v6$^+$ ALL-CM leukemic cells and, after 5 weeks, with nHuSGM3 T cells transduced with a CD19.28z CAR. Mean counts ± s.d. of human CD14$^+$ monocytes before CAR T cell infusion are shown. A one-way ANOVA with Bonferroni correction was used for statistical analysis; ***$P<0.001$ (**a**). Kaplan–Meyer survival plots for the mice are shown. Exact P values from a Mantel–Cox two-sided log-rank test are shown for HuSGM3 F versus HuNSG F (blue; hazard ratio, 3.8; 95% CI, 1.1–13.3) (**b**). **c–e**, Eight-week-old SGM3 mice were co-infused i.v. with HSPCs (HuSGM3, $n=3$ donors) and CD19$^+$CD44v6$^+$ ALL-CM leukemic cells and, after 7 weeks, with nHuSGM3 T cells transduced with a CD19.28z CAR (19.28z, $n=20$ from 2 independent experiments). Three days before CAR T cell infusion, mice were left untreated or were treated with liposomal clodronate (LC, $n=10$ per group). Non-HSPC-humanized SGM3 mice were used as control ($n=10$). Mean temperature change ± s.d. is shown; dashed lines indicate the threshold for high fever ($\Delta T>2$ °C). A two-way ANOVA with Bonferroni correction was used for statistical analysis; ***$P<0.001$ (**c**). Kaplan–Meyer survival plots are shown. Exact P values from a Mantel–Cox two-sided log-rank test are shown for HuSGM3 + LC versus HuSGM3 (red; hazard ratio, 8.3; 95% CI, 0.9–80.5) (**d**). Mean leukemic cells percentages ± s.d. at Day 1 (D1), Day 7 and Day 14 from CD19.28z CAR T cell infusion are shown. A one-way ANOVA with Bonferroni correction was used for statistical analysis; ***$P<0.001$. Percentages are gated on total human CD45$^+$ cells circulating in mouse blood (**e**). **f–h**, HuSGM3 mice were infused i.v. with nHuSGM3 T cells transduced with either a CD44v6.28z CAR (44v6.28z, $n=15$ from 3 independent experiments) or a CD19.28z CAR (19.28z, $n=15$). Three weeks later, mice received 5×10^6 CD19$^+$CD44v6$^+$ ALL-CM leukemic cells. Non-HSPC-humanized SGM3 mice were infused with either nHuSGM3 CD44v6.28z or CD19.28z CAR T cells as control, and results were pooled (44v6/19.28z in SGM3, $n=17$). Mean temperature change ± s.d is shown; dashed lines indicate the threshold for high fever ($\Delta T>2$ °C). A two-way ANOVA with Bonferroni correction was used for statistical analysis; ***$P<0.001$ (**f**). Kaplan–Meyer survival plots are shown. Exact P values from a Mantel–Cox two-sided log-rank test are shown for 19.28z in HuSGM3 versus 28z in SGM3 (blue; hazard ratio, 13.9; 95% CI, 1.8–105.0) (**g**). Mean bone marrow (BM) leukemic cells percentages ± s.d. at 24 weeks after CAR T cell infusion are shown. A one-way ANOVA with Bonferroni correction was used for statistical analysis; ***$P<0.001$. Percentages are gated on total human and mouse CD45$^+$ cells (**h**).

both time points. As expected, cluster 6, comprising both B cells and leukemic cells, was present at the earlier time point, but disappeared later on, mirroring on-target clearance of CD19$^+$ cells. Contrariwise, clusters 1, 8 and 3 (CD4$^+$ and CD8$^+$ T cells) were selectively enriched at day 7, reflecting CAR T cell expansion. At the single-cell level, monocytes specifically expressed high levels of *IL1B* and *IL6* as well as *CXCL8* (*IL8*), *CCL2*, *CCL8* and *CXCL10* (Fig. 5d). Other cell types contributing to inflammatory cytokine production included DCs (Fig. 5d, Supplementary Fig. 17a–h and Supplementary Table 3).

Anakinra protects from lethal neurotoxicity by CAR T cells. In humans, tocilizumab is often used, either alone or in combination with steroids, to manage CAR T cell toxicities; it ameliorates fever and hypotension typical of severe CRS, but apparently fails to revert severe neurotoxicity[7,9,13]. Despite anecdotal reports, definitive data on CRS responsiveness to anakinra, an IL-1 receptor antagonist, are lacking. Motivated by the in vitro observation of early IL-1 induction in monocytes by CAR T cells, we used our xenograft mouse model of human CRS to verify whether anakinra might have some advantages over tocilizumab. At the time of CAR T cell infusion,

© 2018 Nature America Inc., part of Springer Nature. All rights reserved.

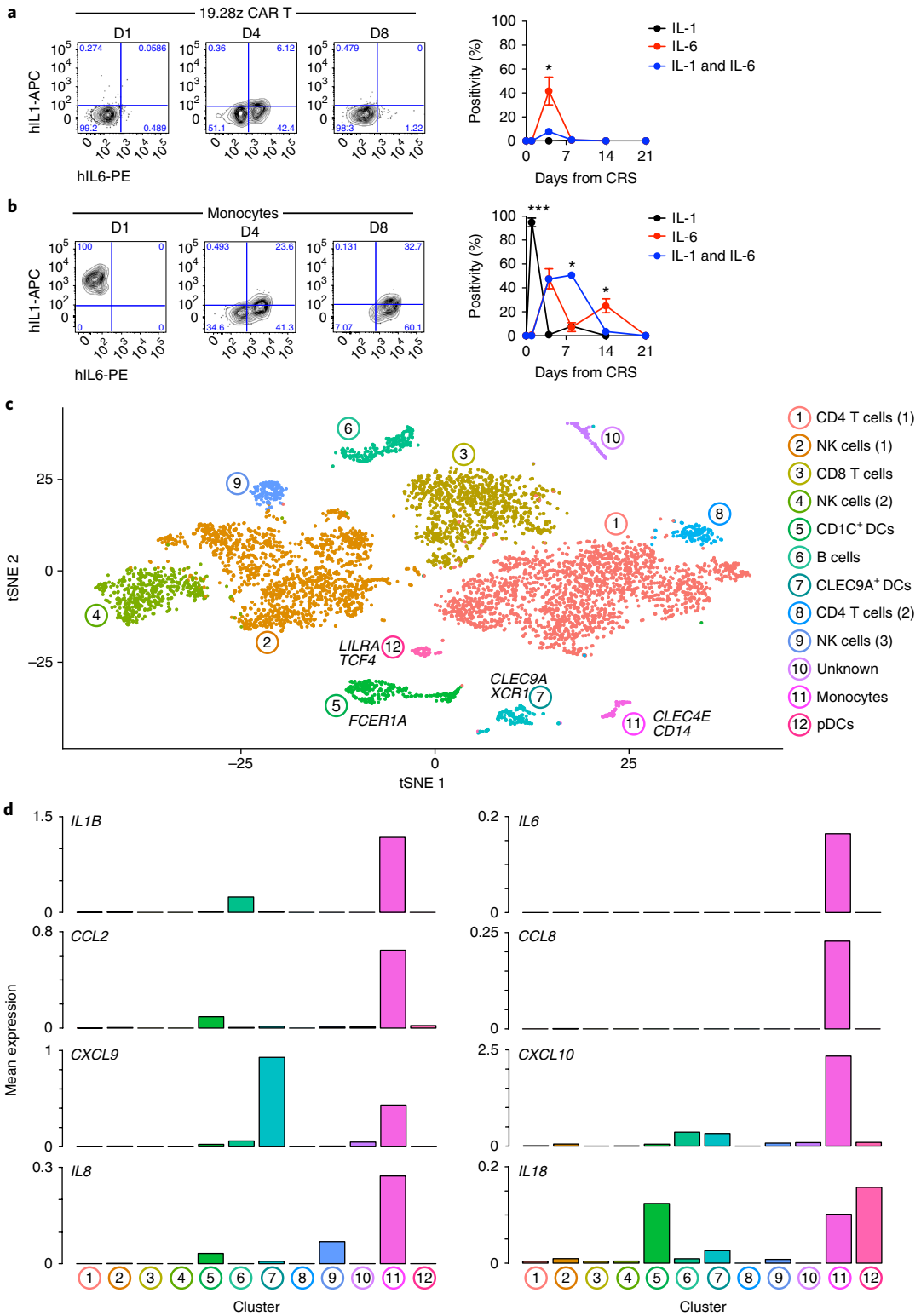

Fig. 5 | Monocytes are key sources for IL-6 and IL-1 during CRS. a,**b**, Eight-week-old SGM3 mice ($n=8$ from 2 independent experiments) were co-infused i.v. with 1×10^5 HSPCs ($n=2$ donors) and 5×10^6 CD19$^+$CD44v6$^+$ ALL-CM leukemic cells and, after 5 weeks, with 2×10^6 T cells from nHuSGM3 transduced with a CD19.28z CAR. Representative plots and mean intracellular human IL-1 and/or IL-6 percentages ± s.d. in circulating CAR T cells (**a**) and monocytes (**b**) are shown. A two-way ANOVA with Bonferroni correction was used for statistical analysis; $^*P<0.05$, $^{***}P<0.001$. **c**, t-distributed stochastic neighbor embedding (tSNE) visualization plot of scRNA-seq data from human CD45$^+$ cells ($n=6{,}511$; sequenced at a median depth of 56,164 reads per cell and with an average number of 1,980 detected genes per cell) from leukemic HuSGM3 mice infused with CD19.28z CAR T cells after 2 and 7 d from fever onset (pooled data). Separated 2- and 7-d tSNE plots are shown in Supplementary Fig. 16f. Numbers and colors highlight transcriptional clusters as related to different subpopulations. Representative discriminative genes are indicated for clusters 5, 7, 11 and 12 (DCs and monocytes). NK cells, natural killer cells; pDCs, plasmacytoid dendritic cells. **d**, Mean expression of the indicated genes for each cluster. The units on the *y* axes are log-transformed unique molecular identifier (UMI) per 10,000 transcripts.

© 2018 Nature America Inc., part of Springer Nature. All rights reserved.

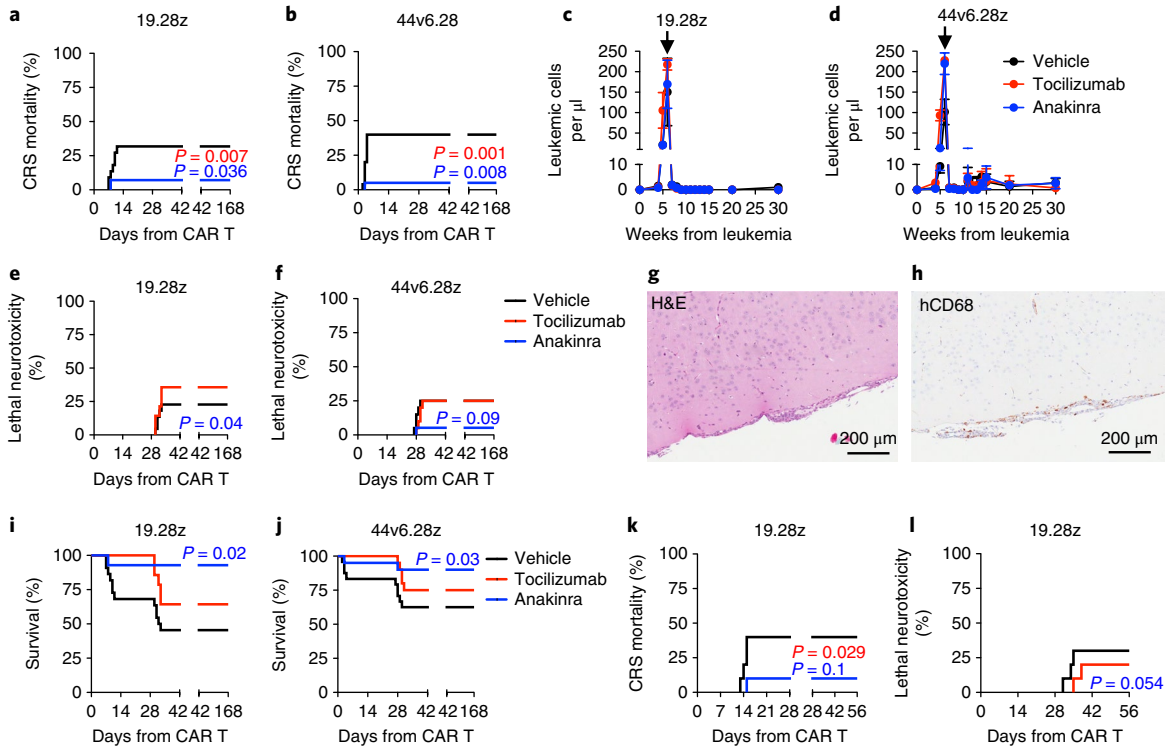

Fig. 6 | Anakinra, but not tocilizumab, abolishes neurotoxicity. Eight-week-old SGM3 mice were co-infused i.v. with HSPCs ($n=5$ donors, HuSGM3) and 5×10^6 CD19$^+$CD44v6$^+$ ALL-CM leukemic cells and, after 7 weeks (for high leukemia burden), with 2×10^6 nHuSGM3 T cells transduced with a CD44v6.28z CAR (44v6.28z, $n=50$ from 3 independent experiments) or a CD19.28z CAR (19.28z, $n=50$). Just before CAR T cell infusion, mice received vehicle ($n=14$ per group), tocilizumab ($n=18$) or anakinra ($n=18$). **a**,**b** CRS mortality curves (see Methods for CRS mortality definition). Exact *P* values from a Mantel–Cox two-sided log-rank test are shown for tocilizumab (red; hazard ratio, 6.4; 95% CI, 1.6–24.7) or anakinra (blue; hazard ratio, 3.9; 95% CI, 1.1–14.4) versus vehicle in mice infused with 19.28z CAR T cells or for tocilizumab (red; hazard ratio, 7.9; 95% CI, 2.2–29.2) or anakinra (blue; hazard ratio, 5.3; 95% CI, 1.5–18.4) versus vehicle in mice infused with 44v6.28z CAR T cells. **c**,**d**, Mean leukemic cells counts ± s.d. Black arrows indicate CAR T cell infusion. **e**,**f**, Lethal neurotoxicity curves (see Methods for lethal neurotoxicity definition). Exact *P* values from a Mantel–Cox two-sided log-rank test are shown for anakinra (blue; hazard ratio, 6.3; 95% CI, 1.1–37.1) versus vehicle in mice infused with 19.28z CAR T cells or for anakinra (blue; hazard ratio, 4.0; 95% CI, 0.8–20.4) versus vehicle in mice infused with 44v6.28z CAR T cells. **g**,**h**, Brain histology (H&E, **g**) and human CD68 immunohistochemistry images (**h**) of a vehicle-treated mouse (representative of $n=4$) dying from neurotoxicity. **i**,**j**, Kaplan–Meyer survival plots are shown. Exact *P* values from a Mantel–Cox two-sided log-rank test are shown for anakinra (blue; hazard ratio, 3.9; 95% CI, 1.2–12.7) versus vehicle in mice infused with 19.28z CAR T cells or for anakinra (blue; hazard ratio, 3.5; 95% CI, 1.0–11.7) versus vehicle in mice infused with 44v6.28z CAR T cells. **k**,**l**, HuSGM3 mice with a high leukemia burden were infused with 5×10^6 nHuSGM3 T cells transduced with a CD19.28z CAR (19.28z, $n=30$ mice). At fever onset, mice received vehicle ($n=10$ per group), tocilizumab ($n=10$ per group) or anakinra ($n=10$ per group). CRS mortality curves are shown. Exact *P* values from a Mantel–Cox two-sided log-rank test are shown for tocilizumab (red; hazard ratio, 9.180; 95% CI, 1.247–67.57) versus vehicle or for anakinra (blue; hazard ratio, 4.343; 95% CI, 0.6998–26.95) versus vehicle (**k**). Lethal neurotoxicity curves are shown. Exact *P* values from a Mantel–Cox two-sided log-rank test are shown for anakinra (blue; hazard ratio, 8.33; 95% CI, 0.8615–80.54) versus vehicle (**l**).

cohorts of leukemic HuSGM3 mice were administered either tocilizumab or anakinra or vehicle as control. Neither drug substantially interfered with in vivo CAR T cell expansion or in vivo IFN-γ and IL-2 production (Supplementary Fig. 18a–f), and both were effective at preventing CRS by both CD19.28z and CD44v6.28z CAR T cells (Fig. 6a,b and Supplementary Fig. 18g–j). CRS prevention by tocilizumab was associated with early normalization and a later increase in systemic human IL-6 levels (Supplementary Fig. 18k–m). Initial normalization of systemic human IL-1 levels by anakinra was not followed by a similar increase (Supplementary Fig. 18n), possibly owing to a different pharmacology in mice than in humans. Systemic human IL-8 and CCL3/MIP-1α levels were protractedly abated following treatment with either drug (Supplementary Fig. 18o–r). Importantly, leukemia clearance by CAR T cells in HuSGM3 mice that received either tocilizumab or anakinra was similar to that in control mice (Fig. 6c,d).

After a median of 30 d (range, 27–33 d) in HuSGM3 mice that prophylactically received either vehicle or tocilizumab, but not in those that received anakinra, we unexpectedly documented the occurrence of a sudden (24-h duration) and lethal neurological syndrome (Fig. 6e,f) characterized by generalized paralysis and, in some cases, by seizures. This form of delayed neurotoxicity was common to both CD19.28z and CD44v6.28z CAR T cell–infused mice and emerged only in mice with previous CRS ($P<0.01$ by Fisher's exact test; data not shown). Postmortem analysis did not reveal any sign of X-GVHD in target organs (skin and liver; data not shown) but conversely showed multifocal brain meningeal thickening without leukemic cell infiltration in the CNS (Fig. 6g). Meningeal thickening that was accompanied by human macrophage infiltration in subarachnoid space, as ascertained by scattered positivity for CD68 by immunohistochemistry (Fig. 6h), was effectively prevented by anakinra but not by tocilizumab (Supplementary Fig. 19a). As a result, only anakinra prophylaxis had a statistically significant effect on overall survival (Fig. 6i). HuSGM3 mice infused with control EGFR.28z CAR T cells did not develop either CRS or neurotoxicity but died from leukemia within 12 weeks (data not shown).

We finally investigated whether administering tocilizumab or anakinra to leukemic HuSGM3 mice after fever onset

© 2018 Nature America Inc., part of Springer Nature. All rights reserved.

(Supplementary Fig. 19b) could revert CRS by CD19.28z CAR T cells. Both drugs were confirmed to be effective at decreasing CRS mortality, although anakinra had borderline statistical significance (Fig. 6k). Nonetheless, anakinra treatment was uniquely associated with rescue from lethal neurotoxicity (Fig. 6l). Leukemia clearance by CAR T cells was unaffected by both treatments (Supplementary Fig. 19c).

Discussion

The cellular and molecular players involved in life-threatening toxicities induced by CAR T cells remain poorly understood. For gauging their pathogenesis, we used T cells derived from HSPC-humanized SGM3 mice, a strain known to better support human lymphohematopoiesis compared to NSG mice[23]. Successful thymic education of human T cells in SGM3 mice was implied by their robust xenotolerance. Although the reasons for efficient human T cell development in this strain are unknown, it is reasonable to suggest that transgenic expression of c-kit ligand (stem cell factor) might be key[24]. Both transgenic expression of HLA molecules[25,26] and cotransplantation of human thymic tissue[27] have been successfully used for boosting thymopoiesis in HSPC-humanized mice and, in the future, would be worth combining with the SGM3 background.

In this study, we demonstrated at the single-cell level that human circulating monocytes, rather than CAR T cells, are primarily responsible for the systemic release of IL-6, which ultimately causes CRS. Interestingly, mouse cytokines, and IL-6 in particular, did not appear to play a substantial role, likely owing to cytokine dysregulation inherited from the NOD background[28]. In humans, circulating monocytes can be divided in different subpopulations according to their ability to phagocytose (classical monocytes, $CD14^+CD16^-$), produce proinflammatory cytokines (intermediate monocytes, $CD14^+CD16^+$) or patrol endothelial integrity (nonclassical monocytes, $CD14^{lo}CD16^-$)[29]. In our model, proinflammatory monocytes as well as DCs were involved in cytokine production, as revealed by in vivo scRNA-seq analysis; this not only underlies unexpected complexities, but also suggests new cellular and molecular targets for therapeutic intervention. As we have used leukemic cells that, besides obvious bone marrow homing, essentially accumulate in the circulation[30], it is reasonable that intravascular leukemia recognition by CAR T cells might have been crucial for proinflammatory licensing of circulating myeloid cells. Although we cannot exclude that in tumors with limited blood recirculation, the role of proinflammatory monocytes could be less prominent, our findings might explain the apparently higher incidence of severe CRS reported in human ALL[7,9,13] as compared to non-Hodgkin lymphoma (NHL)[6,31–33].

Although human T cells are known to produce IL-6, the major sources of this cytokine in vivo are monocytes and macrophages[34]. Confirming recent findings[35], our results show that upon tumor recognition in vitro, CAR T cells produce negligible levels of IL-6, whose release conversely requires bystander monocytes. Quite unexpectedly, however, we also observed that, in the course of proinflammatory monocyte licensing, IL-1 preceded IL-6 production by many hours. As IL-1 is capable of inducing the secretion of IL-6 as well as soluble IL-6R (sIL-6R)[34], it is tempting to speculate that CRS might be primarily initiated by IL-1 release from circulating monocytes. Accordingly, in our model, antagonizing IL-1 by in vivo administration of anakinra was equally effective at protecting mice from CRS mortality as blocking IL-6 signaling with tocilizumab. Most importantly, successful CRS prophylaxis by either drug did not hinder antileukemic efficacy, warranting potential routine adoption in the clinic.

Neurotoxicity by CD19 CAR T cells is becoming an emerging issue[12]. The halt to some CD19 CAR T cell trials for lethal neurotoxicity has emphasized the need for a better understanding of this severe pathology. We were surprised to find that our model of CAR T cell therapy not only faithfully recapitulated CRS but also neurotoxicity. Neurotoxicity by CAR T cells in mice was seemingly unrelated to leukemia recognition in the CNS and was associated with histopathological signs of meningeal inflammation, indicating blood–brain barrier leakage to peripherally produced cytokines, as was recently described in humans[36]. As clinical data are accumulating, it is emerging that neurotoxicity by CAR T cells may be more diversified than initially assumed. Far from asserting that the specific type of neurotoxicity observed in our model may fit all varieties, our findings appear highly clinically relevant. For example, by analogy with humans, tocilizumab did not protect mice from lethal neurotoxicity. In striking contrast, anakinra proved highly effective, revealing that IL-1 is a valuable target for global pharmacological intervention. Selective responsiveness of neurotoxicity to anakinra is supported by data in neonatal-onset multisystem inflammatory disease (NOMID)[37,38], an autoinflammatory disease characterized by chronic aseptic meningitis.

At present, it is debated whether CRS and neurotoxicity are restricted to CD19 CAR T cells or are to be expected with CAR T cells specific for other tumor antigens. We have recently developed a CD44v6 CAR T cell strategy for treating AML and multiple myeloma[17]. Here we show that the same severe toxicities are common to CD44v6 CAR T cells and interestingly found substantial aggravation in case of a BBz design, rather than a 28z design. In contrast to CD44v6.28z CAR T cells, which rapidly ablated circulating monocytes and protected mice from subsequent CRS, CD44v6.BBz CAR T cells paradoxically induced proinflammatory monocyte licensing, resulting in 100% CRS mortality. Although these findings might support the prophylactic infusion of CD44v6.28z CAR T cells soon after hematopoietic stem cell transplantation (HSCT) as a way to prevent toxicities, increased leukemia relapse associated with prolonged monocyte aplasia warrants the implementation of a suicide gene for switching off delayed unwanted effects[17].

In summary, we have demonstrated that monocyte-derived IL-1 and IL-6 are required for CRS and neurotoxicity by CAR T cells and that targeted intervention against IL-1 may successfully overcome both toxicities. Besides the immediate translational consequences of these findings, our model could be used in the future for investigating other issues relevant to engineered cell therapies for cancer and other diseases.

Methods

Methods, including statements of data availability and any associated accession codes and references, are available at https://doi.org/10.1038/s41591-018-0036-4.

Received: 30 July 2017; Accepted: 23 March 2018;
Published online: 28 May 2018

References

1. Brentjens, R. J. et al. Safety and persistence of adoptively transferred autologous CD19-targeted T cells in patients with relapsed or chemotherapy refractory B-cell leukemias. *Blood* **118**, 4817–4828 (2011).
2. Savoldo, B. et al. CD28 costimulation improves expansion and persistence of chimeric antigen receptor-modified T cells in lymphoma patients. *J. Clin. Invest.* **121**, 1822–1826 (2011).
3. Kochenderfer, J. N. et al. B-cell depletion and remissions of malignancy along with cytokine-associated toxicity in a clinical trial of anti-CD19 chimeric-antigen-receptor-transduced T cells. *Blood* **119**, 2709–2720 (2012).
4. Porter, D. L., Levine, B. L., Kalos, M., Bagg, A. & June, C. H. Chimeric antigen receptor-modified T cells in chronic lymphoid leukemia. *N. Engl. J. Med.* **365**, 725–733 (2011).
5. Grupp, S. A. et al. Chimeric antigen receptor-modified T cells for acute lymphoid leukemia. *N. Engl. J. Med.* **368**, 1509–1518 (2013).
6. Neelapu, S. S. et al. Axicabtagene ciloleucel CAR T-cell therapy in refractory large B-Cell lymphoma. *N. Engl. J. Med.* **377**, 2531–2544 (2017).
7. Maude, S. L. et al. Tisagenlecleucel in children and young adults with B-cell lymphoblastic leukemia. *N. Engl. J. Med.* **378**, 439–448 (2018).

© 2018 Nature America Inc., part of Springer Nature. All rights reserved.

8. Davila, M. L. et al. Efficacy and toxicity management of 19-28z CAR T cell therapy in B cell acute lymphoblastic leukemia. *Sci. Transl. Med.* **6**, 224ra25 (2014).
9. Turtle, C. J. et al. CD19 CAR-T cells of defined $CD4^+$:$CD8^+$ composition in adult B cell ALL patients. *J. Clin. Invest.* **126**, 2123–2138 (2016).
10. Turtle, C. J. et al. Durable molecular remissions in chronic lymphocytic leukemia treated with CD19-specific chimeric antigen receptor-modified T cells after failure of ibrutinib. *J. Clin. Oncol.* **35**, 3010–3020 (2017).
11. Teachey, D. T. et al. Identification of predictive biomarkers for cytokine release syndrome after chimeric antigen receptor T-cell therapy for acute lymphoblastic leukemia. *Cancer Discov.* **6**, 664–679 (2016).
12. Lee, D. W. et al. Current concepts in the diagnosis and management of cytokine release syndrome. *Blood* **124**, 188–195 (2014).
13. Park, J. H. et al. Long-term follow-up of CD19 CAR therapy in acute lymphoblastic leukemia. *N. Engl. J. Med.* **378**, 449–459 (2018).
14. Topp, M. S. et al. Safety and activity of blinatumomab for adult patients with relapsed or refractory B-precursor acute lymphoblastic leukaemia: a multicentre, single-arm, phase 2 study. *Lancet Oncol.* **16**, 57–66 (2015).
15. Bondanza, A. et al. Suicide gene therapy of graft-versus-host disease induced by central memory human T lymphocytes. *Blood* **107**, 1828–1836 (2006).
16. Mastaglio, S. et al. NY-ESO-1 TCR single edited central memory and memory stem T cells to treat multiple myeloma without inducing GvHD. *Blood* **130**, 606–618 (2017).
17. Casucci, M. et al. CD44v6-targeted T cells mediate potent antitumor effects against acute myeloid leukemia and multiple myeloma. *Blood* **122**, 3461–3472 (2013).
18. Gattinoni, L., Speiser, D. E., Lichterfeld, M. & Bonini, C. T memory stem cells in health and disease. *Nat. Med.* **23**, 18–27 (2017).
19. Nijmeijer, B. A., Willemze, R. & Falkenburg, J. H. An animal model for human cellular immunotherapy: specific eradication of human acute lymphoblastic leukemia by cytotoxic T lymphocytes in NOD/scid mice. *Blood* **100**, 654–660 (2002).
20. Rongvaux, A. et al. Human hemato-lymphoid system mice: current use and future potential for medicine. *Annu. Rev. Immunol.* **31**, 635–674 (2013).
21. Shultz, L. D. et al. Multiple defects in innate and adaptive immunologic function in NOD/LtSz-scid mice. *J. Immunol.* **154**, 180–191 (1995).
22. Takenaka, K. et al. Polymorphism in Sirpa modulates engraftment of human hematopoietic stem cells. *Nat. Immunol.* **8**, 1313–1323 (2007).
23. Billerbeck, E. et al. Development of human $CD4^+FoxP3^+$ regulatory T cells in human stem cell factor-, granulocyte-macrophage colony-stimulating factor-, and interleukin-3-expressing NOD-SCID IL2Rγ(null) humanized mice. *Blood* **117**, 3076–3086 (2011).
24. Wils, E. J. et al. Stem cell factor consistently improves thymopoiesis after experimental transplantation of murine or human hematopoietic stem cells in immunodeficient mice. *J. Immunol.* **187**, 2974–2981 (2011).
25. Koo, G. C., Hasan, A. & O'Reilly, R. J. Use of humanized severe combined immunodeficient mice for human vaccine development. *Expert Rev. Vaccines* **8**, 113–120 (2009).
26. Strowig, T. et al. Priming of protective T cell responses against virus-induced tumors in mice with human immune system components. *J. Exp. Med.* **206**, 1423–1434 (2009).
27. Lan, P., Tonomura, N., Shimizu, A., Wang, S. & Yang, Y. G. Reconstitution of a functional human immune system in immunodeficient mice through combined human fetal thymus/liver and $CD34^+$ cell transplantation. *Blood* **108**, 487–492 (2006).
28. Bouma, G. et al. NOD mice have a severely impaired ability to recruit leukocytes into sites of inflammation. *Eur. J. Immunol.* **35**, 225–235 (2005).
29. Patel, A. A. et al. The fate and lifespan of human monocyte subsets in steady state and systemic inflammation. *J. Exp. Med.* **214**, 1913–1923 (2017).
30. Bondanza, A. et al. IL-7 receptor expression identifies suicide gene-modified allospecific $CD8^+$ T cells capable of self-renewal and differentiation into antileukemia effectors. *Blood* **117**, 6469–6478 (2011).
31. Kochenderfer, J. N. et al. Chemotherapy-refractory diffuse large B-cell lymphoma and indolent B-cell malignancies can be effectively treated with autologous T cells expressing an anti-CD19 chimeric antigen receptor. *J. Clin. Oncol.* **33**, 540–549 (2015).
32. Turtle, C. J. et al. Immunotherapy of non-Hodgkin's lymphoma with a defined ratio of $CD8^+$ and $CD4^+$ CD19-specific chimeric antigen receptor-modified T cells. *Sci. Transl. Med.* **8**, 355ra116 (2016).
33. Schuster, S. J. et al. Chimeric antigen receptor T cells in refractory B-cell lymphomas. *N. Engl. J. Med.* **377**, 2545–2554 (2017).
34. Hunter, C. A. & Jones, S. A. IL-6 as a keystone cytokine in health and disease. *Nat. Immunol.* **16**, 448–457 (2015).
35. Singh, N. et al. Monocyte lineage-derived IL-6 does not affect chimeric antigen receptor T-cell function. *Cytotherapy* **19**, 867–880 (2017).
36. Gust, J. et al. Endothelial activation and blood-brain barrier disruption in neurotoxicity after adoptive immunotherapy with CD19 CAR-T cells. *Cancer Discov.* **7**, 1404–1419 (2017).
37. Goldbach-Mansky, R. et al. Neonatal-onset multisystem inflammatory disease responsive to interleukin-1β inhibition. *N. Engl. J. Med.* **355**, 581–592 (2006).
38. Fox, E. et al. The serum and cerebrospinal fluid pharmacokinetics of anakinra after intravenous administration to non-human primates. *J. Neuroimmunol.* **223**, 138–140 (2010).

Acknowledgements

We thank G. Dotti (University of North Carolina) and H. Abken (University of Cologne) for providing the original CAR constructs, F. Falkenburg (Leiden University Medical Center) for providing ALL-CM leukemic cells and L. Naldini (San Raffaele-Telethon Institute for Gene Therapy) for providing lentiviral vectors. We thank R. Norato (San Raffaele Scientific Institute) for histology technical support. This work was supported by the Italian Association for Cancer Research (AIRC) (MFAG grant no. 13390 and Investigator grant no. 17706 to B.A.; MFAG grant no. 20247 to O.R.).

Author contributions

M.N. and B.C. designed and performed experiments and interpreted results. M.C. and L.F. assisted in experimental design and provided constructs and vectors. A.P. performed experiments and interpreted results. F.S., M.P., P.C. and C.D. performed histopathological analysis. G.B. and M.G. performed and analyzed scRNA-seq experiments. C.T., C. Bordignon, F.C. and C. Bonini interpreted results. R.O. supervised G.M. and B.G., interpreted results and wrote the manuscript. A.B. designed experiments and interpreted results. M.N. and A.B. wrote the manuscript and prepared the figures. All authors approved the final version of the manuscript.

Competing interests

C.T. and C. Bordignon are employees of Molmed Spa, whose potential product is studied in this work. F.C. and C. Bonini are consultants of Molmed Spa.

Additional information

Supplementary information is available for this paper at https://doi.org/10.1038/s41591-018-0036-4.

Reprints and permissions information is available at www.nature.com/reprints.

Correspondence and requests for materials should be addressed to A.B.

Publisher's note: Springer Nature remains neutral with regard to jurisdictional claims in published maps and institutional affiliations.

© 2018 Nature America Inc., part of Springer Nature. All rights reserved.

Methods

Generation of CAR constructs. CAR constructs were generated by gene synthesis of single-chain fragment variables (scFVs) specific for human CD44v6 (BIWA-8) or CD19 (FMC63) fused to a nerve growth factor receptor–derived spacer (NGFR), a transmembrane domain, a costimulatory endodoman from either CD28 (28z), 4-1BB (BBz) or OX40 (zOX) and the CD3 zeta chain. In case of CD28 endodomains, the transmembrane domain was also derived from CD28. In all other cases, it was derived from CD4. All sequences were of human origin. All constructs were expressed in SFG retroviral vectors. Retroviral supernatants were produced in 293 T cells.

Cells and culture conditions. T cells were derived from the peripheral blood of healthy blood donors after gradient centrifugation. CB mononuclear cells were supplied by commercial vendors (Lonza). All procedures were approved by the Institutional Review Board of San Raffaele University Hospital and Scientific Institute (IRB number, TIGET_01) and were compliant with all relevant ethical regulations. Leukemic cell lines (THP-1, BV173) were purchased from ATCC and cultured in RPMI 1640 (BioWhittaker) with 10% FBS (Lonza). THP-1 leukemia progression was followed in vivo by ultrasound imaging of the liver. The ALL-CM leukemia cell line was derived from the peripheral blood of a patient with chronic myeloid leukemia in lymphoid blast crisis who expresses CD10, CD19 and CD20. ALL-CM leukemic cells were propagated in vitro with X-VIVO (Lonza) and 2% human serum (Euroclone). CD44v6 was inserted in ALL-CM leukemic cells by lentiviral transduction. T cells were activated with CD3/CD28 beads (InVitrogen) at 3:1 ratio, transduced by spinoculation at Day 2 and 3, and cultured in RPMI 1640 10% FBS with IL-7/IL-15 (5 ng/ml, Peprotech)[39]. At Day 6, beads were removed, and transduction efficiency was determined by staining with an anti-NGFR monoclonal antibody reactive with the CAR spacer. T cell expansion is expressed as fold increase (T cell number at Day 15 / T cell number at Day 0). DCs were generated by culturing NSG mouse bone marrow, human peripheral blood or CB mononuclear cell adherent fractions in IMDM 5% FBS with GM-CSF (800 UI/ml, Peprotech) and IL-4 (500 UI/ml) for 6 d, followed by overnight LPS maturation (1 μg/ml, Sigma). Prior to in vivo infusion, DCs received irradiation (10,000 cGy) from a linear accelerator (Gilardoni).

Flow cytometry. Mouse monoclonal antibodies specific for human CD3 (brilliant violet 510 (BV510)-conjugated, clone OKT3, Biolegend, lot no. B226707; allophycocyanin (APC)/Cy7-conjugated, clone SK7, Biolegend, lot no. B225054), CD4 (peridinin chlorophyll protein complex (PerCP)-conjugated, clone SK3, BD Biosciences, lot no. 23-5127-01), CD8 (APC/Cy7-conjugated, clone SK1, Biolegend, lot ni. B209571), CD14 (PerCP-conjugated, clone MΦP9, BD Biosciences, lot ni. 23-5143-01), CD15 (BV510-conjugated, clone W6D3, Biolegend, lot ni. B201379), CD19 (phycoerythrin (PE)-conjugated, clone HIB19, Biolegend, lot no. B188908), CD33 (PE-conjugated, clone WM53, Biolegend, lot no. B195145), CD44v6 (PE-conjugated, clone 2F10, R&D, lot no. YAV0616061; APC-conjugated, clone 2F10, R&D, lot no. YAW0515041), CD45 (APC/Cy7-conjugated, clone HI30, Biolegend, lot no. B214034; PE/Cy7-conjugated, clone HI30, Biolegend, lot no. B210429), CD45RA (FITC-conjugated, clone HI100, Biolegend, lot no. B202186), CD62L (APC-conjugated, clone DREG-56, Biolegend, lot no. B230061), CD95 (PE-conjugated, clone DX2, Biolegend, lot no. B2013943), NGFR (PE-conjugated, clone C40-1457, BD Biosciences, lot no. 7068641), IL-6 (PE-conjugated, Miltenyi Biotec, lot no.5171106502) and IL-1 (APC-conjugated, Miltenyi Biotec, lot no. 5171106567) and a rat monoclonal antibody specific for mouse CD45 (Ly5.1; PerCP-conjugated, clone 30-F11, Biolegend, lot no. B214531) were purchased from commercial vendors. Samples were run through a FACS Canto II flow cytometer (BD Biosciences), and data were analyzed with the FlowJo software (LLC). An example of gating strategy is shown in Supplementary Fig. 1a. HSPCs were sorted with CD34 immunomagnetic beads (Miltenyi), following the manufacturer's recommendations. After sorting, purity was checked using flow cytometry and was confirmed to be > 95%.

In vitro functional assays. CAR T cells were cultured with target cells at different effector to target (E:T) ratios in RPMI 1640 and 10% FBS. After 24–48 h, coculture supernatants were collected and subsequently analyzed with the LEGENDplex bead-based cytokine immunoassay (Biolegend). After 4 d, surviving cells were counted and analyzed using flow cytometry. T cells transduced with an irrelevant CAR (EGFR-specific) were always used as control. Elimination index was calculated as follows: 1 – (number of residual target cells in presence of experimental CAR-T cells) / (number of residual target cells in presence of control CAR T cells). In CFSE dilution assays, T cells were loaded with CFSE (Thermofisher) and stimulated with irradiated (10,000 cGy) splenocytes from NSG or CD57/Bl6 mice or with irradiated human allogeneic peripheral blood mononuclear cells at an effector to stimulator (E:S) ratio of 1:5. After 6 d, T cell proliferation was measured using flow cytometry. Monocyte-like cell differentiation was induced in THP1 cells through 48 h of treatment with PMA (Sigma, 50 nM). Primary autologous monocytes were isolated from human peripheral blood mononuclear cells with CD14 immunomagnetic beads (Miltenyi) and cultured in RPMI 1640 and 10% FBS.

Mouse experiments. All mouse experiments were approved by the Institutional Animal Care and Use Committee (IACUC) of San Raffaele University Hospital and Scientific Institute and by the Italian Governmental Health Institute (Rome, Italy). Mice were kept in a specific-pathogen-free (SPF) facility within individually ventilated cages and were given irradiated food and water ad libitum. 6- to 8-week-old female or male NSG (NOD.Cg-Prkdc^{scid} Il2rgt^{m1Wjl}) or SGM3 (NSG Tg$^{CMV\text{-}IL3,CSF2,KITLG}$1Eav/MloySzJ; Jackson Laboratories) mice were screened using PCR (according to JAX instructions and primers, stock no. 013062) and ELISA (R&D systems; catalog nos. DCK00, DGM00 and D3000 for SCF, GM-CSF and IL-3, respectively) for transgene expression and human cytokine expression. Newborn (0–2 d from birth) female of male NSG or SGM3 mice were sublethally irradiated (150 cGy from a linear accelerator) and intrahepatically injected with 1×10^5 human CB CD34$^+$ cells. Adult mice were sublethally irradiated (200 cGy) and immediately i.v. infused with 1×10^5 human CB CD34$^+$ cells. For assessing X-GVHD, mice were monitored daily for hunching, activity, fur texture, skin integrity and weight loss. For studying CAR T cell toxicities, mice were assessed daily for weight loss and for body temperature by rectal thermometry and weekly for mouse SAA concentration by ELISA, for uric acid by enzymatic test and for human cytokine concentration by LegendPLEX (Biolegend). CRS mortality was defined as death preceded by the following criteria: > 15% body weight loss, $\Delta T > 2$ °C and serum IL-6 > 1,500 pg/ml. Lethal neurotoxicity was defined as death in the absence of CRS criteria and preceded by either paralysis or seizures. For evaluating antileukemia efficacy, mice were infused i.v. with THP-1 (1×10^6) or ALL-CM (5×10^6 or 10×10^6 for mice in Fig. 2) leukemic cells and, after 5 or 7 weeks (low or high tumor burden, respectively), with 2×10^6 CAR T cells. Leukemic and CAR T cell counts were monitored weekly in peripheral blood by FACS using Flow-Count Fluorospheres (BeckmanCoulter). Mice were euthanized when weight loss was > 20% or when signs of inhumane suffering manifested. For depleting phagocytes, mice were treated intraperitoneally (i.p.) with liposomal clodronate (http://www.clodronateliposomes.com/) for three consecutive days before CAR T cell infusion. Tocilizumab (10 mg per kg body weight, Roactemra, Roche) or anakinra (10 mg per kg body weight, Kineret, Amgen) were administered i.v. immediately before CAR T cells. Although tocilizumab was given only once, anakinra administration was repeated daily for 7 d because of the different pharmacokinetics.

Single-cell RNA sequencing. scRNA-seq libraries were generated using a microfluidics-based approach[40]. Droplet-based digital 3′ scRNA-seq was performed on a Chromium Single-Cell Controller (10x Genomics, Pleasanton, CA) using the Chromium Single Cell 3′ Reagent Kit v2 according to the manufacturer's instructions. Briefly, suspended single cells were partitioned in Gel Beads in Emulsion (GEMs) and lysed, and this was followed by RNA barcoding, reverse transcription and PCR amplification (12–14 cycles). Sequencing-ready scRNA-seq libraries were prepared according to the manufacturer's instructions, checked and quantified on 2100 Bioanalyzer (Agilent Genomics, Santa Clara, CA) and Qubit 3.0 (Invitrogen, Carlsbad, CA) instruments. Sequencing was performed on a NextSeq 500 machine (Illumina, San Diego, CA) using the NextSeq 500/550 High Output v2 kit (75 cycles).

Single-cell RNA sequencing data analysis. RNA-seq data have been deposited in the ArrayExpress database at EMBL-EBI (http://www.ebi.ac.uk/arrayexpress/) under accession number E-MTAB-6505. Raw reads were processed and aligned to the hg19 transcriptome using CellRanger v1.3 (10 × Genomics) with default parameters. Reads were aligned to reference genome hg19, and gene expression levels were quantified using ENSEMBL genes as the gene model. Only confidently mapped reads that were non-PCR duplicates with valid barcodes and unique molecular identifiers (UMIs) were retained to compute a gene expression matrix containing the number of UMIs for each cell and gene. Gene counts were imported in the R environment (v3.3.2) and processed with Seurat v2.1 (http://satijalab.org/seurat/). Cells expressing less than 500 unique genes were discarded. Counts were normalized using Seurat function NormalizeData with default parameters. Cells with a ratio of mitochondrial versus endogenous genes expression exceeding 0.1 were also excluded. Expression data were than scaled using ScaleData function, regressing on number of UMIs, percentage of mitochondrial gene expression and cell cycle S and G2M scores (calculated using the CellCycleScoring function).

Graph-based clustering. Most variable genes across the dataset were identified using FindVariableGenes function; genes with an average expression lower than 0.01 and higher than 3 were excluded, and a cutoff of 0.5 was applied over dispersion z-scores. The first 30 principal components were then evaluated on the resulting 1,175 genes. Cell clusters were then defined at resolution $r = 0.2$ using FindCluster function and visualized in 2-dimensions using t-SNE[41,42]. Discriminative genes among clusters were identified among those expressed in at least 10% of cells within the cluster and ranked by decreasing fold change, computed comparing the mean expression between cluster cells and all the other cells.

Histopathological analysis. After H&E staining, mouse organs, including thymus and brain, were blindly and independently analyzed by at least two pathologists

© 2018 Nature America Inc., part of Springer Nature. All rights reserved.

(S.F. and C. P.) who were experienced with NSG mice. Immunohistochemistry for human CD3 or CD68 was performed according to standard procedures. Meningeal thickening was scored according to the following arbitrary criteria: 0, normal; 1, mild; 2, moderate; 3, severe.

Statistics. Statistical analysis was performed using a one- or two-way ANOVA, a Mantel–Cox (log-rank) test or a two-tailed Mann–Whitney test (Prism Software 5.0, GraphPad). Differences with a P value < 0.05 were considered statistically significant. Sample size was calculated through power analysis with 0.05 alpha error and 0.80 power. For experiments on antileukemia efficacy (assumptions: leukemia progression in 100% of control mice versus 50% in treated mice), power analysis returned a $n = 11$ size per experimental group. For experiments on tocilizumab or anakinra effectiveness (assumptions: CRS mortality in 35% of control mice versus 0% in treated mice), power analysis returned a $n = 17$ size per experimental group. Before any treatment, mice were blindly randomized, and no sample or animal was excluded from analysis.

Reporting Summary. Further information on experimental design is available in the Nature Research Reporting Summary linked to this article.

Data availability. All relevant data are included in the manuscript and/or in its supplementary information files. RNA-seq data have been deposited in the ArrayExpress database at EMBL-EBI (http://www.ebi.ac.uk/arrayexpress/) under accession number E-MTAB-6505. CAR sequences are available upon request to the corresponding author. NGFR-derived CAR spacer sequences are detailed in the patent application WO2016042461 A1.

References

39. Kaneko, S. et al. IL-7 and IL-15 allow the generation of suicide gene-modified alloreactive self-renewing central memory human T lymphocytes. *Blood* **113**, 1006–1015 (2009).
40. Zheng, G. X. et al. Massively parallel digital transcriptional profiling of single cells. *Nat. Commun.* **8**, 14049 (2017).
41. Levine, J. H. et al. Data-driven phenotypic dissection of AML reveals progenitor-like cells that correlate with prognosis. *Cell* **162**, 184–197 (2015).
42. Villani, A. C. et al. Single-cell RNA-seq reveals new types of human blood dendritic cells, monocytes, and progenitors. *Science* **356**, eaah4573 (2017).

© 2018 Nature America Inc., part of Springer Nature. All rights reserved.

nature research

Corresponding author(s): Attilio Bondanza

Life Sciences Reporting Summary

Nature Research wishes to improve the reproducibility of the work that we publish. This form is intended for publication with all accepted life science papers and provides structure for consistency and transparency in reporting. Every life science submission will use this form; some list items might not apply to an individual manuscript, but all fields must be completed for clarity.

For further information on the points included in this form, see Reporting Life Sciences Research. For further information on Nature Research policies, including our data availability policy, see Authors & Referees and the Editorial Policy Checklist.

Please do not complete any field with "not applicable" or n/a. Refer to the help text for what text to use if an item is not relevant to your study.
For final submission: please carefully check your responses for accuracy; you will not be able to make changes later.

Experimental design

1. Sample size

Describe how sample size was determined.

Sample size was calculated by a professional biostatistician by power analysis (Rosner B. Fundamentals of biostatistics.7th Edition Boston, MA. Brooks/Cole, 2011) and was approved by the Institutional Animal Care and Use Committee (IACUC) of San Raffaele Hospital Scientific Institute (Milan, IT) and by the Italian Governmental Health Institute (Rome, IT). A statement on results of sample-size calculation by power analysis has been included in the Methods section.

2. Data exclusions

Describe any data exclusions.

No data were excluded from analysis in each experiment.

3. Replication

Describe the measures taken to verify the reproducibility of the experimental findings.

All attempts at replication were successful in each experiment.

4. Randomization

Describe how samples/organisms/participants were allocated into experimental groups.

Mice were allocated to experimental groups randomly.

5. Blinding

Describe whether the investigators were blinded to group allocation during data collection and/or analysis.

Technicians performing infusions into mice, sampling, preparation and flow cytometry analysis were blinded to experimental groups.

Note: all in vivo studies must report how sample size was determined and whether blinding and randomization were used.

6. Statistical parameters

For all figures and tables that use statistical methods, confirm that the following items are present in relevant figure legends (or in the Methods section if additional space is needed).

n/a	Confirmed
☐	☒ The exact sample size (*n*) for each experimental group/condition, given as a discrete number and unit of measurement (animals, litters, cultures, etc.)
☐	☒ A description of how samples were collected, noting whether measurements were taken from distinct samples or whether the same sample was measured repeatedly
☐	☒ A statement indicating how many times each experiment was replicated
☐	☒ The statistical test(s) used and whether they are one- or two-sided *Only common tests should be described solely by name; describe more complex techniques in the Methods section.*
☐	☒ A description of any assumptions or corrections, such as an adjustment for multiple comparisons
☐	☒ Test values indicating whether an effect is present *Provide confidence intervals or give results of significance tests (e.g. P values) as exact values whenever appropriate and with effect sizes noted.*
☐	☒ A clear description of statistics including central tendency (e.g. median, mean) and variation (e.g. standard deviation, interquartile range)
☐	☒ Clearly defined error bars in all relevant figure captions (with explicit mention of central tendency and variation)

See the web collection on statistics for biologists for further resources and guidance.

Software

Policy information about availability of computer code

7. Software

Describe the software used to analyze the data in this study.	Prism Software 5, GraphPad. CellRanger v1.3 (10X Genomics). https://support.10xgenomics.com/single-cell-gene-expression/software/pipelines/latest/what-is-cell-ranger R environment (v3.3.2). https://www.r-project.org Seurat v2.1. http://satijalab.org/seurat/

For manuscripts utilizing custom algorithms or software that are central to the paper but not yet described in the published literature, software must be made available to editors and reviewers upon request. We strongly encourage code deposition in a community repository (e.g. GitHub). *Nature Methods* guidance for providing algorithms and software for publication provides further information on this topic.

Materials and reagents

Policy information about availability of materials

8. Materials availability

Indicate whether there are restrictions on availability of unique materials or if these materials are only available for distribution by a third party.	No unique material was used.

9. Antibodies

Describe the antibodies used and how they were validated for use in the system under study (i.e. assay and species).	Mouse monoclonal Abs specific for human CD3 (BV510-conjugated, clone OKT3, Biolegend, lot nr. B226707, Cat 317332, dilution 1:100; APC-Cy7-conjugated, clone SK7, Biolegend, lot nr. B225054, Cat 344818, dilution 1:100), CD4 (PerCP-conjugated, clone SK3, BD Biosciences, lot nr. 23-5127-01, Cat 344624, dilution 1:100); CD8 (APC-Cy7-conjugated, clone SK1, Biolegend, lot nr. B209571, Cat 344714, dilution 1:100); CD14 (PerCP-conjugated, clone M P9, BD Biosciences, lot nr. 23-5143-01, Cat 345786, dilution 1:50); CD15 (BV510-conjugated, clone W6D3, Biolegend, lot nr. B201379, Cat 323028, dilution 1:100); CD19 (PE-conjugated, clone HIB19, Biolegend, lot nr. B188908, Cat 302208, dilution 1:100); CD33 (PE-conjugated, clone WM53, Biolegend, lot nr. B195145, Cat 303404, dilution 1:100); CD44v6 (PE-conjugated, clone 2F10, R&D, lot nr. YAV0616061, Cat FAB3660P, dilution 1:50; APC-conjugated, clone 2F10, R&D, lot nr. YAW0515041, Cat FAB3660A, dilution 1:50); CD45 (APC-Cy7-conjugated, clone HI30, Biolegend, lot nr. B214034, Cat 304014, dilution 1:200; PE-Cy7-conjugated, clone HI30, Biolegend, lot nr. B210429, Cat 304016, dilution 1:200); CD45RA (FITC-conjugated, clone HI100, Biolegend, lot nr. B202186, Cat 304106, dilution 1:100), CD62L (APC-conjugated, clone DREG-56, Biolegend, lot nr. B230061, Cat 304810, dilution 1:100); CD95 (PE-conjugated, clone DX2, Biolegend, lot nr. B2013943, Cat 305608, dilution 1:100); NGFR (PE-conjugated, clone C40-1457, BD Biosciences, lot nr. 7068641, Cat 557196, dilution 1:50); IL-6 (PE-conjugated, clone MQ2-13A5, Miltenyi Biotec, lot nr.5171106502, Cat 130-096-086, dilution 1:50); IL-1 (APC-conjugated, clone 364-3B3-14, Miltenyi Biotec, lot nr. 5171106567, Cat 130-109-227, dilution 1:50), and a rat mAb specific for mouse CD45 (Ly5.1; PerCP-conjugated, clone 30-F11, Biolegend, lot nr. B214531, Cat 103130, dilution 1:200) were purchased from commercial vendors. Samples were run through a FACS Canto II flow cytometer (BD Biosciences) and data were analyzed with the FlowJo software (LLC). Prior to use, all antibodies were validated and titrated on human peripheral blood and cord blood mononuclear cells or on mouse peripheral blood.

10. Eukaryotic cell lines

a. State the source of each eukaryotic cell line used.	Cell lines were purchased from ATCC. Patient-derived ALL-CM leukemic cells were kindly provided by Fred Falkenburg (Leiden University Medical Center, The Netherlands). 293T packaging cells were kindly provided by Luigi Naldini (Telethon Institute, San Raffaele, Milano IT).
b. Describe the method of cell line authentication used.	No cell line was authenticated. Prior to use, each cell line was however validated for surface antigen expression by flow cytometry and for xeno-engraftment in NSG mice (take, latency, biodistribution in relevant organs).
c. Report whether the cell lines were tested for mycoplasma contamination.	All cell lines were routinely tested for mycoplasma contamination by PCR and proved negative.
d. If any of the cell lines used are listed in the database of commonly misidentified cell lines maintained by ICLAC, provide a scientific rationale for their use.	No commonly misidentified cell line was used.

Animals and human research participants

Policy information about studies involving animals; when reporting animal research, follow the ARRIVE guidelines

11. Description of research animals

Provide all relevant details on animals and/or animal-derived materials used in the study.

Eight-to-ten weeks old female or males NSG (NOD.Cg-Prkdcscid Il2rgtm1Wjl) or SGM3 mice (NSG TgCMV-IL3,CSF2,KITLG1Eav/MloySzJ) were purchased from Jackson Laboratories.

Policy information about studies involving human research participants

12. Description of human research participants

Describe the covariate-relevant population characteristics of the human research participants.

The study did not involve human research participants.

nature research

Corresponding author(s): Attilio Bondanza

☐ Initial submission ☐ Revised version ☒ Final submission

Flow Cytometry Reporting Summary

Form fields will expand as needed. Please do not leave fields blank.

Data presentation

For all flow cytometry data, confirm that:

☒ 1. The axis labels state the marker and fluorochrome used (e.g. CD4-FITC).

☒ 2. The axis scales are clearly visible. Include numbers along axes only for bottom left plot of group (a 'group' is an analysis of identical markers).

☒ 3. All plots are contour plots with outliers or pseudocolor plots.

☒ 4. A numerical value for number of cells or percentage (with statistics) is provided.

Methodological details

5. Describe the sample preparation.	Human peripheral blood or cord blood mononuclear cells were isolated by density gradient centrifugation, washed extensively with PBS 2% BSA and stained at 4°C for 20min. Before acquisition, mouse peripheral blood, bone-marrow and spleen single-cell suspensions were treated with ACK solution to lyse red blood cells.
6. Identify the instrument used for data collection.	BD FACSCanto II, BD Biosciences
7. Describe the software used to collect and analyze the flow cytometry data.	FlowJo Software, LLC
8. Describe the abundance of the relevant cell populations within post-sort fractions.	In each experiment, at least 20,000 human CD3+ or CD45+ events were acquired.
9. Describe the gating strategy used.	Mouse peripheral blood, bone-marrow or spleen single-cell suspensions were serially gated as follows: FSC-A/FSC-H, then FSC-A/SSC-A, then human CD45/Ly5.1, then human CD3/CD19 (or any other relevant combination). Beckman-Coulter Flow-Count fluorospheres were gated as follows: FSC-A/FSC-H, then Pacific Blue/PE relevant fluorescence channel.

Tick this box to confirm that a figure exemplifying the gating strategy is provided in the Supplementary Information. ☒